ACS OMEGA

http://pubs.acs.org/journal/acsodf

Article

Green Synthesis of Soy Protein Nanocomposites: Effects of Cross-Linking and Clay Nanoparticles on the Mechanical Performance

Marta Bukartyk, Oksana Zholobko, and Xiang-Fa Wu*

Cite This: *ACS Omega* 2022, 7, 5883−5893

Read Online

ACCESS | Metrics & More | Article Recommendations

ABSTRACT: A green synthesis scheme was adopted for preparation of soy-protein-based clay nanocomposites, in which soy protein isolates (SPIs) were utilized as the biodegradable resin and clay nanoparticles (CNPs) were used as the nanoreinforcing phase. Cross-linking of the SPIs was realized through an aqueous reaction scheme with oxidized sugars (e.g., glucose and sucrose as the typical constituents of soy flours) as the cross-linkers. Toughening effects of the cross-linkers, process parameters, and CNPs on the mechanical properties (e.g., tensile strength, stiffness, strain at break, and toughness) of the resulting SPI-based clay nanocomposites were examined by micromechanical tensile testing. The cross-linking and toughening mechanisms of the SPI-based nanocomposites were evaluated by Fourier transform infrared spectroscopy, sol−gel and color characterization, scanning differential calorimetry, and transmission electron microscopy. Thermal stability of the cross-linked SPIs was evaluated by thermogravimetric analysis. Experimental results show that cross-linking can noticeably improve both the tensile strength and tensile modulus of the resulting SPI films, and a small quantity of CNPs can obviously alter the mechanical properties of the resulting clay nanocomposite films. The present study indicates that defatted soy flours can be directly utilized for developing low-cost, SPI-based nanocomposites without the need for external plasticizers, and the entire synthesis is completely green without involvement of any petroleum-based organic solvents, polymers, and metallic catalysts. Such biodegradable SPI-based green nanocomposites have the potential to substitute fossil-based plastics and polymer composites for use in various industrial products and house utilities.

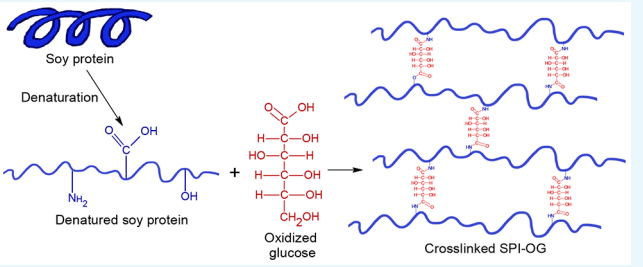

INTRODUCTION

Soybeans represent one of the key agricultural crops in the world, used mainly for extracting soy oils and feeding animals and humans. According to the Department of Agriculture of the United States (USDA), in 2020, U.S. farmers produced 112 million metric tons (4.14 billion bushels) of soybeans, and the production is projected to be up to 120 million metric tons (4.43 billion bushels) in 2021.[1] Such a huge amount of soybeans produced at relatively low costs eagerly demands greatly expanding markets and development of new value-added products beyond their traditional use in oil extraction and foods. In fact, soybeans as sustainable agricultural products can be used as one of the important industrial source materials to potentially substitute the increasing portion of non-renewable petroleum oils, coals, and other minerals for producing environmentally friendly, carbon-neutral, and biodegradable products, which can maintain and improve our lives while significantly reducing the emission of greenhouse gases and deterioration of water, soils, and atmosphere. In the past several decades, significant efforts have been devoted to exploring the promising applications of soy oils and soy meals for various products to substitute their counterparts that are produced from nonrenewable materials. So far, many soy-based products are available in today's market, such as biodiesels, foams, wood/paper adhesives, paints, inks, solvents, lubricants, resins, etc., which are derived principally from soy oils.[2,3]

However, soy-meal (e.g., soy proteins)-based industrial products are not as popular as soy-oil-based products though they occupy over 70 wt % of the soybeans. In many cases, soy meals are only treated as byproducts of soy oil industries with less usage. Different from petroleum-based polymers that have well-defined molecular structures, synthesis routes, and characterization methods that have been accumulated over one century, relatively less research has been done on soy meals that consist of mixture of soy proteins and carbohydrates with a large range and variation of molecular weights and structures. Soy meal as a vastly available solid material is expected to be a fundamental, biodegradable, and sustainable source material substitute for petroleum-based polymers for

Received: October 26, 2021
Accepted: January 31, 2022
Published: February 11, 2022

producing extensive plastic products.[4,5] Recent increasing research efforts are focused on developing various soy-protein-based wood adhesives and coatings via blending soy flours with a variety of plasticizers, such as glycerol, ethylene glycol, polyethylene glycol, propylene glycol, 1,3-propanediol, hyperbranched polyesters, epoxies, etc.[6−10]

Knowledge of the synthesis of soy-oil-based adhesives is valuable. Nevertheless, technical efforts are still needed to develop low-cost, soy-meal-based biodegradable green composites with acceptable mechanical (e.g., tensile strength, stiffness, toughness, etc.) and other physical properties (e.g., thermal stability, gas/vapor permeability, etc.) to satisfy the needs in surface coatings, packaging materials, and bulk structural plastic composites with market viabilities. For instance, reduction and even elimination of the use of external plasticizers, organic solvents, and other fossil-based materials and rare-earth metals can significantly simplify the synthesis process and suppress the fabrication costs for producing soy-flour-based green composites, which can switch the traditional fabrication of structural composites to completely green manufacturing based on low-cost, sustainable agricultural products. In addition, improvement of the mechanical strength, toughness, thermal stability, and vapor/gas impermeability of soy-flour-based composites at low cost is highly desired to greatly expand their practical applications in broad industrial sectors and house utilities (e.g., furniture, exterior and interior building materials, etc.).

Soy proteins as the main constituent of soy flours are long-chain polymer molecules with multiple reactive groups (e.g., −OH, −SH, −COOH, $-NH_2$, etc.), which can be cross-linked with proper small or large molecular weight plasticizers.[6−15] In addition, defatted soy flours contain several water-soluble sugars, such as glucose, fructose, sucrose, raffinose, stachyose, etc., which can be oxidized into aldehydes and carboxylic acids as promising plasticizers to cross-link soy proteins in aqueous solutions without seeking extra external plasticizers.[16] In this process, the soy proteins can be filtrated from low-cost defatted soy flours after being dissolved in water, and the residual soy flour extract in water (i.e., the soluble sugars) can be converted into the reactive plasticizers after oxidation using hydrogen peroxide (H_2O_2) as the oxidant. This is a purely green synthesis process without involving fossil-based organic solvents and polymers as well as without emission of harmful greenhouse gases and wastes. The resulting cross-linked soy proteins with a controllable cross-linking degree are biodegradable resins that can be used for developing structural composites. Compared to their counterparts of fossil/petroleum-based polymeric resins, cross-linked soy proteins carry relatively low mechanical properties. Thus, additional toughening strategies are still needed to achieve low-cost soy-flour-based green composites into the mainstream of structural materials. Among others, exfoliated clay nanoparticles (CNPs) are low-cost nanoreinforcing materials with excellent toughening effects in the mechanical strength and stiffness as well as other physical properties.[17−22] Theoretical studies have elucidated the toughening mechanisms of exfoliated CNPs in polymeric resins due mainly to their high surface area and aspect ratio, excellent tensile and interfacial shear strength, and controllable alignment.[23−30] CNPs provide promising opportunities to toughen cross-linked soy proteins for developing low-cost, high-strength, soy-protein-based green nanocomposites.

In this experimental study, a green synthesis scheme was utilized to oxidize soy-based sugars (i.e., glucose and sucrose) in aqueous solutions for the purpose of cross-linking soy protein isolates (SPIs), which were used as an ideal material model for preparing SPI-oxidized sugar (OS) nanocomposite films. Three SPI/sugar mass ratios of 1:0.25, 1:0.50, and 1:0.75 were considered to examine their effects on the cross-linking and the resulting mechanical properties of the SPI-OS films at proper curing conditions and CNP reinforcement. Detailed Fourier transform infrared (FTIR) spectroscopy as well as color and sol−gel tests were used to characterize the cross-linking of the SPI-OS samples. These characterization results were further correlated to the mechanical properties and thermal stability of the SPI-OS films, which were determined by microtensile mechanical testing, thermogravimetric analysis (TGA), and differential scanning calorimetry (DSC). Detailed discussions of the cross-linking mechanisms, mechanical properties, and thermal stability of the resulting SPI-OS films and their counterparts reinforced with CNPs, as well as their dependencies upon various material and process factors, are made. Conclusions of the present studies are drawn in consequence.

EXPERIMENTAL SECTION

Materials. Soy protein isolate powder was purchased from the NOW Foods (Bloomingdale, IL). Sodium hydroxide (NaOH) was purchased from the VWR International (Radnor, PA). The 30% hydrogen peroxide (H_2O_2), 37% hydrochloric acid (HCl), glucose, sucrose, and nanoclay powders (Nanomer I.28E, montmorillonite clay surface modified with 25−30 wt % trimethyl stearyl ammonium) were purchased from the MilliporeSigma (Burlington, MA). All chemicals and materials were used as received without further purification.

Oxidation of Glucose and Sucrose. The sugars (glucoses or sucroses) were oxidized in an aqueous solution of H_2O_2. In a typical test, 3 g of glucose or sucrose was mixed with 12 g of 7.5 and 15 wt % aqueous H_2O_2 solutions in 25 mL glass vials. In each case, the pH value of the resulting mixture was adjusted to ∼3.0 using 0.1 M HCl, followed by the oxidation reaction for 3 h (glucose) or 6 h (sucrose) at 60 °C and continuous magnetic stirring.

Preparation of Aqueous Solution of Denatured SPIs. Five grams of SPI powder was dissolved in 45 g of deionized water at pH 10 (adjusted using 1 M NaOH) in a 100 mL glass breaker. SPI powder was then denatured for 40 min at 70 °C with continuous stirring to open up the SPI molecules and expose their reactive functional groups (e.g., −OH, −SH, −COOH, $-NH_2$, etc.).

Preparation of SPI Films Cross-Linked with Oxidized Sugars (SPI-OS Films). The mass ratios of SPIs to glucose or sucrose were set as 1:0.25, 1:0.50, and 1:0.75. The denatured SPI solution (36, 30, or 28 g) was mixed with oxidized glucose or sucrose solution (4.5, 7.5, or 10.5 g, respectively) to form SPI-OS solutions in 50 mL glass vials. After addition of the oxidized sugars, the pH value of the mixture dropped and was then adjusted back to pH 10 using 1.0 M NaOH solution to trigger the cross-linking reaction. The obtained mixture was stirred at room temperature for 30 min and then left aside for a sufficient amount of time to remove significant bubbles that were generated after addition of the oxidized sugar solution. Furthermore, the SPI-OS solution was cast onto a Teflon-coated plate using a drawdown bar (Paul N. Gardner Co., Pompano Beach, FL) with adjustable wet layer thickness. The

https://doi.org/10.1021/acsomega.1c06002
ACS Omega 2022, 7, 5883−5893

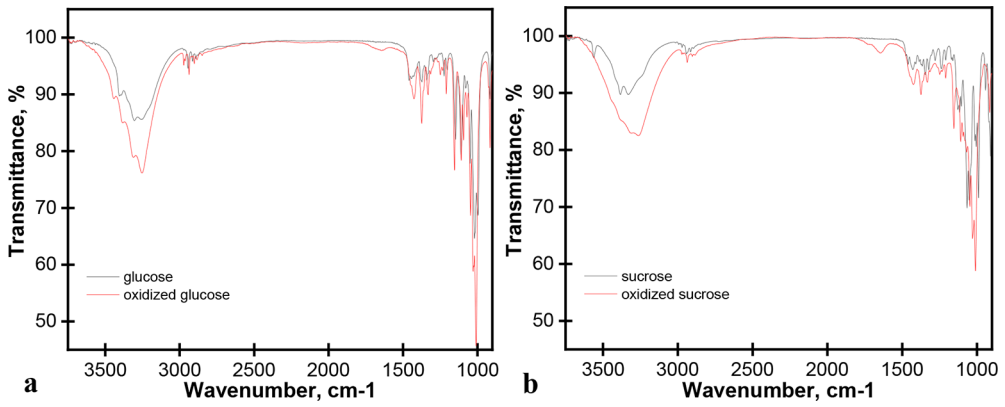

Figure 1. FTIR spectra of pure and oxidized sugars: (a) glucose and (b) sucrose.

resulting cast films were dried in air at room temperature for 40 h. Part of the air-dried film samples were directly used for characterization as uncured film samples. Furthermore, to complete the cross-linking process, the remaining film samples were further cured in an air-circulated oven at 120 °C for 30 min for further characterization as cured film samples.

Preparation of CNP-Reinforced SPI-OS Nanocomposite Films. The nanocomposite films reinforced with CNPs were fabricated according to the same SPI-OS mass ratios of 1:0.25, 1:0.50, and 1:0.75, with addition of 5 wt % of CNPs with respect to the SPIs. During the process, CNP powders (0.17, 0.15, or 0.14 g) were added to the as-prepared solutions of SPIs and oxidized sugar with the targeted pH value. The obtained mixture was vigorously stirred using an analog vortex mixer (Cole-Parmer, Vernon Hills, IL) for about 10 min, followed by continuous magnetic stirring at room temperature for over 7 h. The resulting mixtures of SPI-OS and CNPs were solution-cast onto a Teflon-coated plate to form the wet SPI-OS nanocomposite films, which were dried at room temperature first and then further cured in an air-circulated oven at 120 °C for 30 min. For the purpose of a comparative study, both uncured (with partial SPI cross-linking) and cured (with the maximum cross-linking) nanocomposite film samples were used for characterization and mechanical testing.

FTIR Characterization. FTIR spectra were collected using a Nicolet Fourier transform infrared spectrometer with a Smart iTR attenuated total reflectance sampling accessory (Thermo Fisher Scientific, Waltham, MA). The FTIR spectra were recorded as the average of 64 scans in the range from 600 to 4000 cm^{-1} at the resolution of 4 cm^{-1} with CO_2 and H_2O compensation.

Film Color Characterization. Color change due to the Maillard reaction in the films before and after curing can be used to characterize the cross-linking process that was measured using a BYK Spectro2guide spectrophotometer (BYK-Gardner USA, Columbia, MD). To do so, the L (lightness: "0" indicating black and "100" indicating white), a ("−" indicating greenness and "+" indicating redness), and b ("−" indicating blueness and "+" indicating yellowness) values were measured as the average of at least three measurements for each film sample. The color difference between the uncured and cured film samples, ΔE, was calculated as

$$\Delta E = [(\Delta L^*)^2 + (\Delta a^*)^2 + (\Delta b^*)^2]^{1/2}$$

where ΔL^*, Δa^*, and Δb^* are defined as the differences of lightness, greenness/redness, and blueness/yellowness, respectively, between the uncured and cured samples such that $\Delta L^* = L^*_1 - L^*_2$, $\Delta a^* = a^*_1 - a^*_2$, and $\Delta b^* = b^*_1 - b^*_2$.

Sol−Gel Characterization. Preweighed SPI-OS film samples (uncured and cured) were added separately into two glass vials, each of which was filled with 15 mL of deionized water and stirred using a magnetic stirrer on a hot plate at 80 °C and 100 rpm for 24 h. Then the solid residuals of the mixture in each vial were filtered using Whatman #1 filter paper (Scientific Filters, North Bend, OH) and dried in an air-circulated oven at 120 °C for 45 min. The gel fraction was calculated as the mass ratio of the samples after and before the sol−gel test.

Thermogravimetric Analysis. A TGA test was performed using a thermogravimetric analyzer TGA550 (TA Instruments, New Castle, DE). In each test, the tested sample was heated from room temperature to 600 °C at the heating rate of 10 °C/min under a nitrogen atmosphere (flow rate: 60 mL/min).

Differential Scanning Calorimetrical Characterization. DSC characterization was performed using a TA Q1000 differential scanning calorimeter (TA Instruments, New Castle, DE) with nitrogen as the purge gas. The heating−cooling−heating cycle in the ramping temperature range from −10 to 230 °C (with the heating/cooling rate of 10 °C/min) was used. The glass transition temperature (T_g) was extracted from the second heating cycle.

Transmission Electron Microscopy (TEM) Characterization. TEM characterization of the typical CNP-reinforced SPI-OS nanocomposite films after curing was conducted using a JEOL JEM-2100 analytical TEM to examine the CNP morphology and distribution in the SPI-OS films. During the process, a small piece of the SPI-OS sample (~10 mm × 10 mm) was cut from the SPI-OS film sample and glued onto a glass slide with a transparent thermoplastic glue, from which tiny TEM samples with the areal size of ~1.5 mm × 0.5 mm were cut for the characterization.

Mechanical Characterization. An Instron 5542 tensile tester (Instron Inc., Norwood, MA) installed with a computerized digital data acquisition system (with the maximum load-carrying capacity of 100 N) was employed for characterizing the mechanical properties of the SPI-OS films. Rectangular microtensile test specimens with the areal size of 10 mm × 70 mm and a thickness of 50−100 μm were scissored cautiously from the film samples; adhesive tabs (cut from a 3M Scotch foam mounting double-sided tape) with the areal size of 10 mm × 10 mm were firmly attached onto the two ends at two sides of each microtensile test specimen to

https://doi.org/10.1021/acsomega.1c06002
ACS Omega 2022, 7, 5883−5893

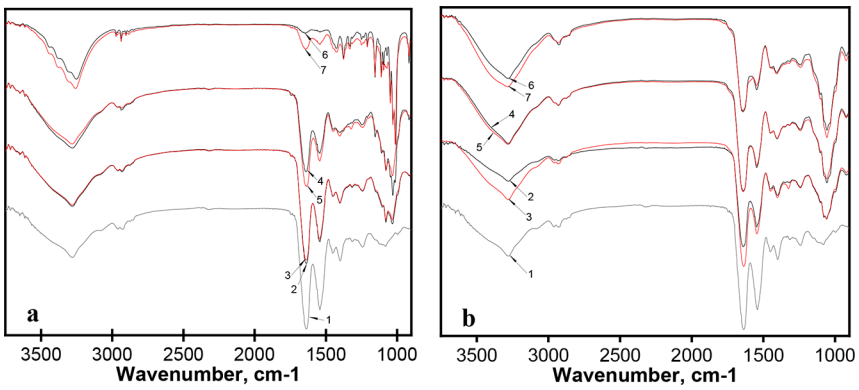

Figure 2. FTIR spectra of SPIs and uncured and cured SPI-OS films: (a) glucose, (b) sucrose. (1) SPI films; (2) SPI/sugar mass ratio = 1:0.25 (uncured); (3) SPI/sugar mass ratio = 1:0.25 (cured); (4) SPI/sugar mass ratio = 1:0.50 (uncured); (5) SPI/sugar mass ratio = 1:0.5 (cured); (6) SPI/sugar mass ratio = 1:0.75 (uncured); (7) SPI/sugar mass ratio = 1:0.75 (cured).

Scheme 1. Schematic Representation of the Maillard Reaction between Carboxyl Groups of Oxidized Sugar and Amino Groups of Soy Protein

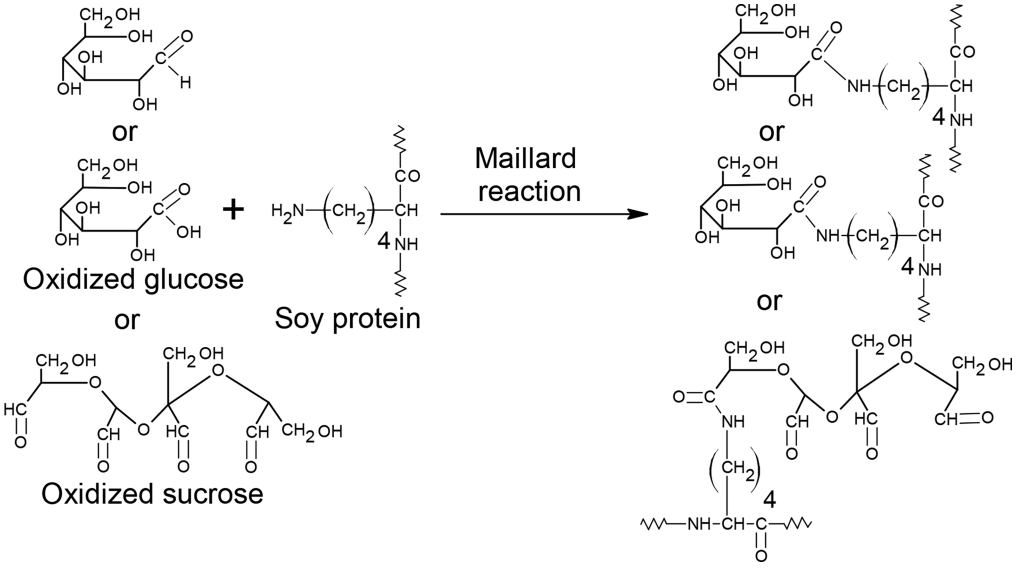

avoid the premature failure to appear at the fixture regions. Thus, the nominal/effective areal size of the microtensile test specimens was 10 mm × 50 mm. During a uniaxial tensile test, a displacement control method with the constant loading rate of 2 mm/min was maintained and at least three specimens were tested in each case of the SPI-OS film specimens.[31−34]

RESULTS AND DISCUSSION

SPI-OS Film Characterization. Figure 1a,b shows the FTIR spectra of the pure and oxidized sugars (glucose (Figure 1a), sucrose (Figure 1b)). Both glucose and sucrose do not contain carbonyl groups in their structures. After oxidation in acidified H_2O_2 solution, the appearance of the peaks at 1710 cm^{-1} (for glucose) and 1720 cm^{-1} (for sucrose), which are correlated to the carbonyl groups, confirms the oxidation of the primary alcohol groups in the glucose and sucrose into carboxylic acids and/or aldehydes. In addition, the oxidation of sugars with acidified H_2O_2 can also be verified by the evidence that a sharp decrease in the pH value to about 1.0 was observed in the mixture during the oxidation process.

Figure 2 shows the FTIR spectra of SPIs and SPI-oxidized glucose films (uncured and cured) with the SPI/sugar ratio of 1:0.50. The SPI spectrum shows three major peaks at 1635, 1540, and 1243 cm^{-1}, which can be assigned to amide I (C═O stretching), amide II (N−H bending, C−N stretching), and amide III (C−N stretching and N−H vibration) bands of proteins, respectively.[35,36] During the oxidation of glucose or sucrose, carboxylic acids can also be formed.[37] These acids can be cross-linked with SPIs via forming ester, anhydride, or amide linkages. The weak ester peaks at 1740 cm^{-1} were detected from the spectra, corresponding to the SPI-OS films with either oxidized glucose or sucrose. Formation of the new amide and imine linkages due to the cross-linking reaction between proteins and sugars was difficult to track as these linkages could coexist in the proteins, and their corresponding peaks overlapped in the fingerprint region. In addition, Figure 2 also indicates that the intensity of these peaks increased after the films were cured, which evidences the formation of new linkages therein. The difference in intensity is increasing with the increase of sugar mass fraction in nearly all of the film samples. The highest difference in the peak intensity between the uncured and cured SPI-oxidized sucrose films appears at the SPI/sugar mass ratio of 0.25, which is in agreement with

https://doi.org/10.1021/acsomega.1c06002
ACS Omega 2022, 7, 5883−5893

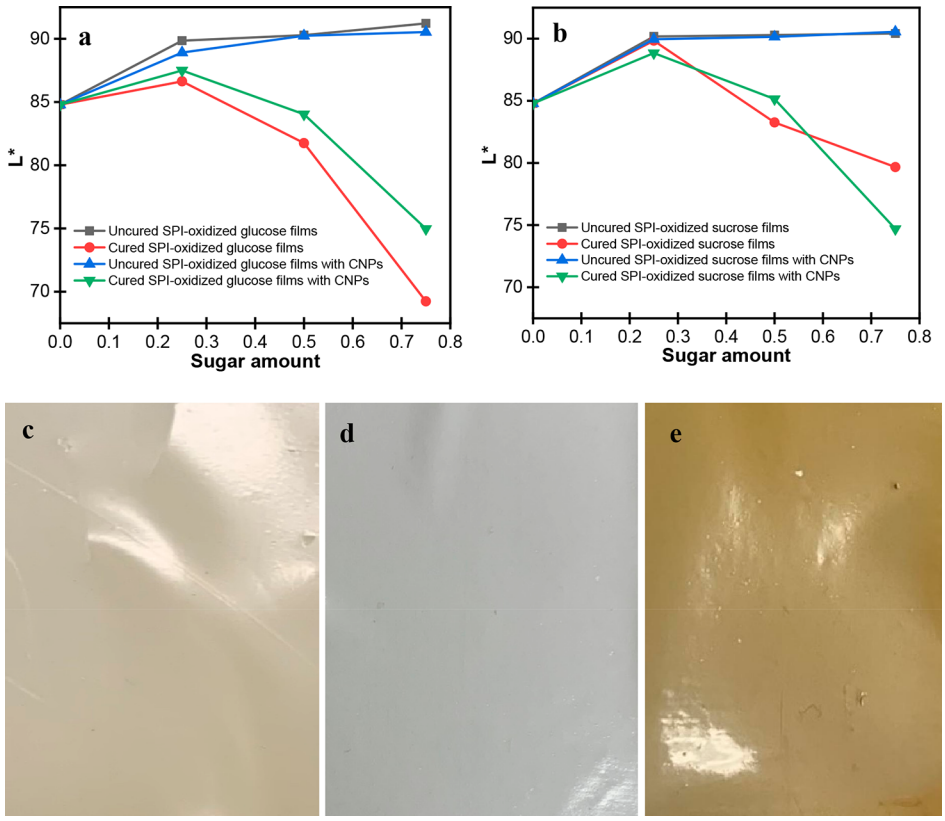

Figure 3. (Top) Lightness differences between uncured and cured SPI-OS films: (a) SPI-oxidized glucose films and (b) SPI-oxidized sucrose films with varying sugar mass fraction (without and with CNPs). (Bottom) Optical images of the films: (c) SPI film, (d) uncured SPI-OS film, and (e) cured SPI-OS film.

the gel fraction of the SPI-oxidized sucrose films compared to those SPI-OS film samples with higher sugar mass fractions.

Formation of the imine linkage due to reaction of the aldehyde groups with amine groups, that is, the Maillard reaction (Scheme 1), can be evidenced by the color change in the films. The lightness differences in the films made of SPIs and oxidized sugars (either glucose or sucrose) at varying sugar mass fraction can be observed in Figure 3. Both glucose and sucrose showed the similar color changes. Due to the Maillard reaction, the color of the film samples changed from the pale yellow (beige) to brownish orange with the progression of the reaction. In the CIE $L^*a^*b^*$ color system, the L^* value corresponds to the color lightness. With decreasing L^* value, the color became darker. Addition of the oxidized sugar to the SPI films led to the lightening of the film color (Figure 3c,d). The L^* value increases from ∼85 to 90%. It can be found that the sugar mass fraction did not significantly influence the color change of the uncured SPI-OS film samples. However, the cross-linked film samples did show the color difference compared to those uncured ones (Figure 3e). The film samples looked darker with increasing sugar mass fraction from 0.25 to 0.75, that is, from ∼90 to 70% for the SPI-oxidized glucose samples (Figure 3a) and 80% for the SPI-oxidized sucrose sample (Figure 3b). Furthermore, addition of CNPs to the samples resulted in darkening of the film samples with the change of L^* value from ∼90 down to 74% for both the SPI-oxidized glucose and SPI-oxidized sucrose samples. Thus, the experimental observations confirm the cross-linking reaction between the aldehyde groups, which were obtained from oxidation of glucose or sucrose and the amine groups from the denatured SPIs.

Table 1 summarizes the color differences between uncured and cured (cross-linked) film samples at three different sugar contents. It can be found that the color difference of either the glucose- or the sucrose-based system increases with increasing sugar content at the given film composition. These experimental results can be rationally explained by the degree of cross-linking between the SPIs and the oxidized sugar, that is, the higher mass fraction of sugar, the higher concentration of the reactive centers presented in the system, resulting in the higher cross-linking degree. In addition, the color differences in the SPI-oxidized glucose film samples are higher than those of the SPI-oxidized sucrose film samples, corresponding to the results of the sol−gel characterization (Table 2).

Table 1. Color Differences between Uncured and Cured SPI-OS Film Samples at Different Sugar Mass Fractions (without and with CNP Reinforcement)

	SPI-oxidized glucose films			SPI-oxidized sucrose films		
sugar mass fraction	0.25	0.50	0.75	0.25	0.50	0.75
ΔE (without CNPs)	15.46	36.78	75.05	1.05	27.07	39.74
ΔE (with CNPs)	6.73	24.10	60.66	5.20	18.68	53.09

Experimental results of the sol−gel test are summarized in Table 2. Pure SPI films and uncured SPI-oxidized glucose films completely disintegrated in water after a certain time. However, cross-linked SPI-OS films as well as uncured SPI-oxidized sucrose film samples demonstrated partial disintegration. However, cured SPI-oxidized glucose film samples showed the gel fractions of 24, 35, and 32% for the SPI to

https://doi.org/10.1021/acsomega.1c06002
ACS Omega 2022, 7, 5883−5893

Table 2. Gel Mass Fraction for SPI-OS Films at Three Different Sugar Mass Fractions (with and without CNP Reinforcement)[a]

	SPI-oxidized glucose films			SPI-oxidized sucrose films					
sugar mass fraction	0.25	0.50	0.75	0.25		0.50		0.75	
	cured	cured	cured	uncured	cured	uncured	cured	uncured	cured
gel fraction, % (without clay nanoparticles)	23.9 ± 3.1	34.9 ± 1.6	31.8 ± 1.2	37.1 ± 0.1	43.8 ± 0.3	31.1 ± 0.2	35.0 ± 1.5	26.8 ± 0.1	29.2 ± 0.3
gel fraction, % (with clay nanoparticles)	5.5 ± 0.3	32.2 ± 2.3	35.0 ± 0.4	30.9 ± 6.4	47.0 ± 6.4	25.2 ± 7.2	34.9 ± 0.5	33.7 ± 0.5	35.7 ± 0.2

[a]Uncured SPI-oxidized glucose films were completely dissolved in water.

Scheme 2. Schematic Illustration of the Possible SPI-Oxidized Glucose Network Formation

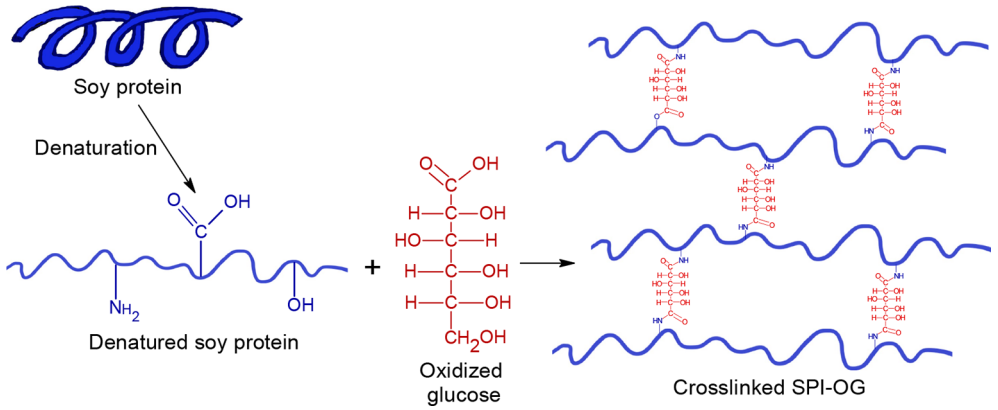

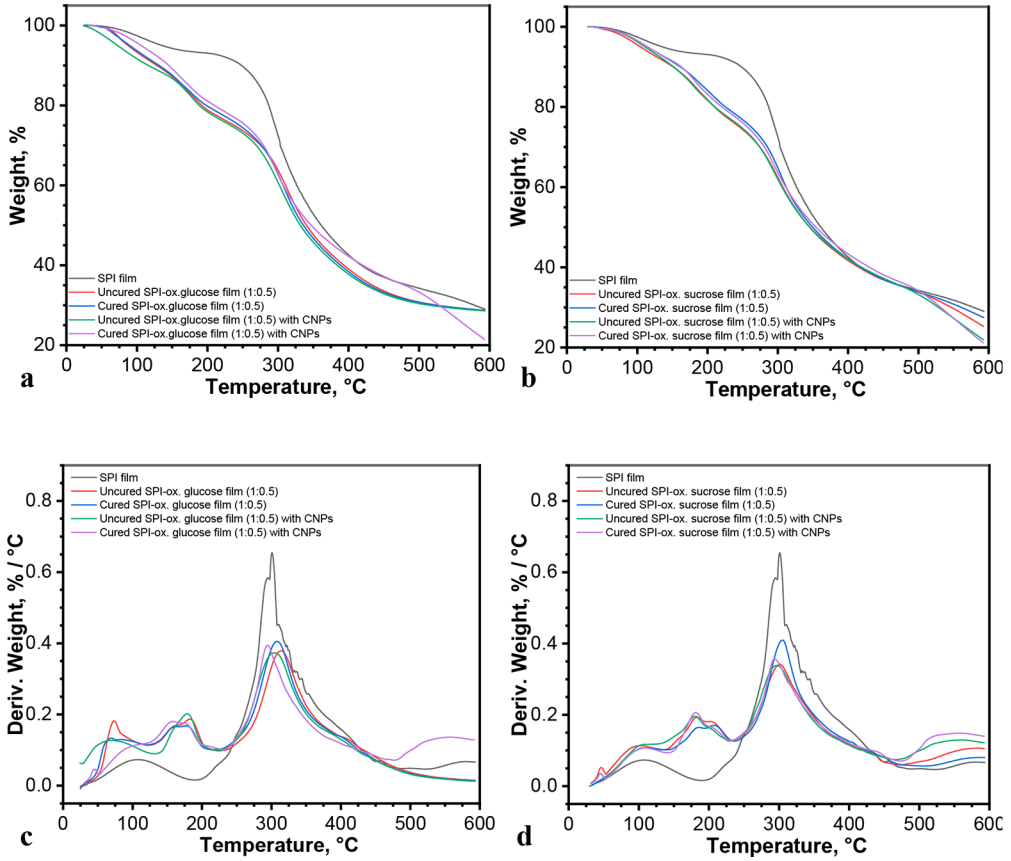

Figure 4. TG (top) and DTG (bottom) diagrams of SPI and SPI-OS films (with and without CNPs): (a,c) SPI-oxidized glucose films and (b,d) SPI-oxidized sucrose films.

sugar mass ratios of 1:0.25, 1:0.50, and 1:0.75, respectively, which is the direct experimental evidence to endorse that curing enhances the cross-linking of SPIs and related improvement of the mechanical properties of the resulting

https://doi.org/10.1021/acsomega.1c06002
ACS Omega 2022, 7, 5883−5893

SPI-OS films. Furthermore, the sol−gel test also indicates that addition of the higher amount of oxidized sugar did not significantly influence the gel fraction at the given curing conditions. To be mentioned, all of the film samples were cured in an air-circulated oven at 120 °C for 30 min, which resulted in the similar cross-linking degree in each film sample.

Interestingly, the uncured SPI-oxidized sucrose samples showed ∼30% of gel fraction at all the SPI to sugar mass ratios under this investigation, indicating the evidence that the cross-linking reaction between SPIs and oxidized sucrose started at room temperature. Compared to the glucose molecule, sucrose is a dimer with a longer chain that is capable of forming the larger number of reactive centers during the oxidation reaction. Therefore, the length of the molecule and the amount of functional groups possibly contribute to the differences of the gel fraction. In addition, the gel fraction of SPI-oxidized sucrose samples increased after curing in the oven. However, the gel residual of the films made of SPI-oxidized sucrose with the sugar mass fraction of 0.25 is higher than that of the rest of the samples with the higher sugar mass fractions, which indicates the higher cross-linking degree of the sucrose-based system with the lower sugar amount. Similar trends were also observed for CNP-reinforced film samples, indicating that CNPs did not significantly affect the cross-linking of the films. The schematic representation of the possible formation of cross-linked SPI-oxidized glucose films is shown in Scheme 2.

Effects of cross-linking and addition of CNPs on the thermal stability of the resulting SPI-OS films were investigated using TGA. Figure 4 shows the thermogravimetric (TG) and derivative thermogravimetric (DTG) diagrams of both the SPI-oxidized glucose and sucrose film samples. Pure SPI films demonstrated two peaks in the DTG diagram (Figure 4c,d). A small weight loss of 6.7% is observed in the temperature range from 25 to 150 °C, corresponding to the moisture loss. After the heating temperature was higher than 225 °C, the weight loss became significant and reached ∼71.7% of the total weight loss of the sample at 600 °C. These results are in good agreement with those reported in the literature.[38,39] In addition, the SPI-OS films showed similar thermogravimetric profiles, almost independent of glucose or sucrose in the films (uncured and cured). Similar to SPI films, a small weight loss of 7−10% in the temperature range from 25 to 150 °C was observed due to the moisture loss. Appearance of the second peak at ∼180 °C in the DTG diagrams of the SPI-OS films is attributed to the loss of bound water.[40,41] According to the TG and DTG diagrams, the loss of free and bound water ended at approximately 200 °C for SPI-oxidized glucose films and 225 °C for SPI-oxidized sucrose films. Thermal decomposition of the SPI-OS films began at the temperature ∼225 °C with T_{max} at ∼ 300 °C for uncured SPI-oxidized sucrose films and 314 °C for uncured SPI-oxidized glucose films. Cross-linking of the SPI-OS films resulted in a small shift of T_{max} toward 305 and 308 °C, respectively. Addition of CNPs to the system resulted in the decrease of T_{max} to 304 °C for uncured SPI-oxidized glucose films and 296 °C for uncured SPI-oxidized sucrose film samples. Similarly, cross-linking resulted in a small decrease of T_{max} to 294 and 293 °C for SPI-oxidized glucose and sucrose film samples, respectively. The total percentage of residues after heating to 600 °C was about 27−28%.

DSC characterization was further used to study the thermal transitions of the SPIs and the uncured and cured SPI-OS films (with and without CNP reinforcement). The thermograms are shown in Figure 5. The glass transition temperature (T_g) is the

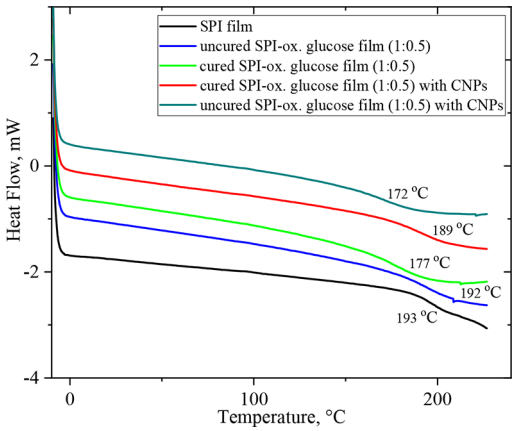

Figure 5. DSC thermograms of the SPI and SPI-oxidized glucose films (with and without CNP reinforcement).

second-order event and can be observed as a slight change in the slope of the curve. The value of T_g in polymeric systems can vary due to several factors including the molecular weight, changes in tacticity, retained monomer, degree of cross-linking, mobility, and interaction of the polymeric matrix with filler.[42−44] Addition of glucose to the system did not noticeably alter T_g (193 °C for the SPI films and 192 °C for the uncured SPI-oxidized glucose films), whereas curing of the films leads to the decrease in T_g to 177 °C. Addition of glucose to the SPIs can lead to the plasticizing effect. Incorporation of the glucose increased the free volume between the SPI chains, which facilitated the mobility of the system. A similar trend was observed for the CNP-reinforced nanocomposite films. However, in the case of CNPs, the decrease of the T_g value is even more pronounced (172 and 189 °C for the uncured and cured samples, respectively), indicating the higher impact of the incorporation of CNPs into the SPI-OS films.

Mechanical Properties. Figure 6 shows the typical tensile stress−strain diagrams of the SPI-OS film samples (with and without CNP reinforcement) in three cases of the sugar mass fraction (i.e., 0.25, 0.50, and 0.75) under this experimental investigation. Tables 3 and 4 tabulate the corresponding ultimate tensile strength, Young's modulus (tangential modulus at initial loading), strain at break, and toughness of the SPI-OS film samples. Figures 7 and 8 are the optical images of the typical uncured and cured microtensile test film specimens before and after testing. For either SPI-oxidized glucose or SPI-oxidized sucrose film specimens, both the ultimate tensile strength and Young's modulus decreased abruptly with increasing sugar mass fraction in the case of either uncured or cured film samples. In the case of uncured SPI-oxidized glucose films without CNP reinforcement, the average ultimate tensile strengths are 15.46, 3.61, and 0.68 MPa corresponding to the SPI/glucose mass ratios of 1:0.25, 1:0.50, and 1:0.75 of the films, respectively. In contrast, after curing, the average ultimate tensile strengths of these films became 17.58, 7.13, and 3.80 MPa, respectively. The average Young's moduli are 574.29, 169.32, and 24.46 MPa for uncured SPI-oxidized glucose films with the SPI/glucose mass ratios of 1:0.25, 1:0.50, and 1:0.75, respectively. After curing, these average moduli increased to 872.09, 247.31, and 124.88 MPa, respectively. Such observations indicate that, given an SPI/glucose mass ratio, curing enhanced both the ultimate tensile strength and Young's modulus of the resulting SPI-oxidized glucose films, however, with much more noticeable

https://doi.org/10.1021/acsomega.1c06002
ACS Omega 2022, 7, 5883−5893

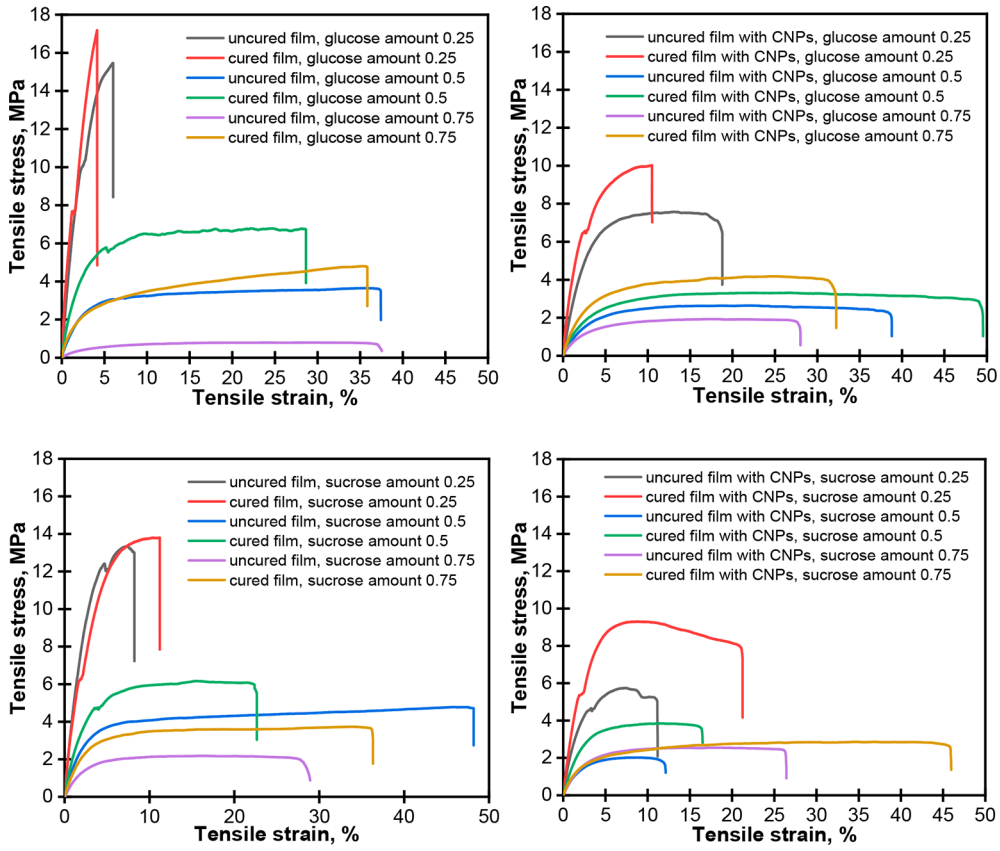

Figure 6. Typical tensile stress−strain diagrams of uncured and cured SPI-oxidized glucose/sucrose films at varying sugar mass fractions (without and with CNP reinforcement).

Table 3. Mechanical Properties of Uncured and Cured SPI-OS Films at Three Different Sugar Mass Fractions

	SPI-oxidized glucose films						SPI-oxidized sucrose films					
sugar mass fraction	0.25		0.50		0.75		0.25		0.50		0.75	
	uncured	cured	uncured	cured	uncured	cured	uncured	cured	uncured	cured	uncured	cured
tensile strength, MPa	15.46 ± 0.77	17.58 ± 0.63	3.61 ± 0.38	7.13 ± 0.42	0.68 ± 0.03	3.80 ± 0.48	14.58 ± 1.73	13.81 ± 1.43	5.07 ± 0.47	5.30 ± 0.12	1.67 ± 0.30	3.07 ± 0.81
strain at break, %	6.03 ± 0.30	4.22 ± 0.19	38.95 ± 6.55	32.68 ± 7.59	36.72 ± 4.07	34.77 ± 3.15	8.27 ± 1.73	11.19 ± 1.00	19.66 ± 3.14	27.24 ± 3.92	30.26 ± 2.79	36.99 ± 3.30
Young's modulus, MPa	574.29 ± 28.71	872.09 ± 154.94	169.32 ± 18.96	247.31 ± 22.08	24.46 ± 1.31	124.88 ± 15.31	565.05 ± 74.86	502.40 ± 58.43	193.13 ± 10.70	253.76 ± 25.34	88.43 ± 6.91	138.03 ± 7.08
toughness, $J \cdot m^{-3}$	62.93 ± 3.15	44.18 ± 1.28	138.14 ± 18.96	209.93 ± 57.27	26.79 ± 2.99	117.96 ± 15.81	89.85 ± 16.77	122.35 ± 11.23	95.19 ± 19.99	153.87 ± 29.80	58.73 ± 5.41	122.05 ± 16.30

Table 4. Mechanical Properties of Uncured and Cured SPI-OS Films at Three Different Sugar Mass Fractions (with CNP Reinforcement)

	SPI-oxidized glucose films with CNPs						SPI-oxidized sucrose films with CNPs					
sugar mass fraction	0.25		0.50		0.75		0.25		0.50		0.75	
	uncured	cured	uncured	cured	uncured	cured	uncured	cured	uncured	cured	uncured	cured
tensile strength, MPa	6.80 ± 0.98	9.57 ± 0.52	2.00 ± 0.18	2.28 ± 0.43	1.67 ± 0.17	3.79 ± 0.40	4.20 ± 0.46	7.12 ± 0.40	1.48 ± 0.52	3.54 ± 0.27	2.26 ± 0.21	2.93 ± 0.24
strain at break, %	15.36 ± 4.30	10.00 ± 2.34	39.92 ± 8.55	51.36 ± 8.78	27.66 ± 2.07	31.04 ± 0.93	12.60 ± 0.95	21.32 ± 1.47	12.13 ± 1.92	18.12 ± 3.16	26.26 ± 1.92	46.27 ± 6.94
Young's Modulus, MPa	272.73 ± 26.90	431.00 ± 12.74	82.16 ± 2.95	100.54 ± 16.22	65.82 ± 5.00	134.29 ± 12.38	301.72 ± 4.82	368.54 ± 33.41	102.79 ± 10.54	167.67 ± 3.52	100.26 ± 10.52	110.39 ± 3.52
toughness, $J \cdot m^{-3}$	94.97 ± 27.67	75.84 ± 19.88	87.85 ± 19.66	160.15 ± 42.91	47.68 ± 5.14	111.38 ± 8.95	70.77 ± 11.59	169.14 ± 17.35	19.77 ± 7.39	64.45 ± 13.85	60.58 ± 6.46	139.33 ± 30.44

https://doi.org/10.1021/acsomega.1c06002
ACS Omega 2022, 7, 5883−5893

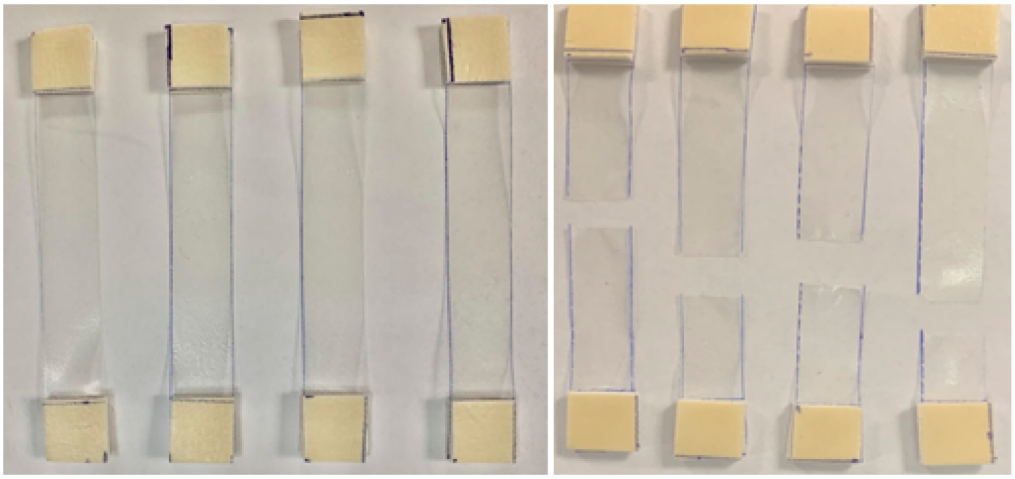

Figure 7. Uncured SPI-OS film specimens before (left) and after (right) uniaxial tension test.

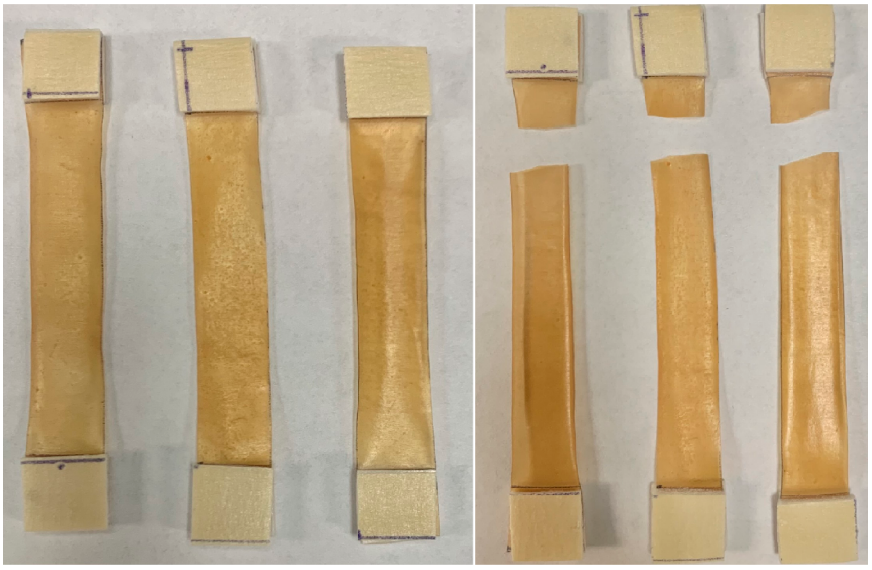

Figure 8. Cured SPI-OS film specimens before (left) and after (right) uniaxial tension test.

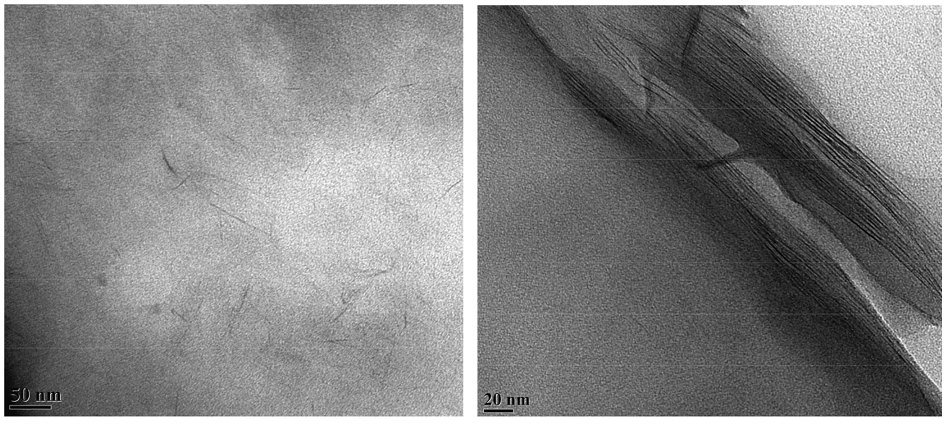

Figure 9. Typical TEM micrographs of a cured SPI-oxidized glucose film sample reinforced with CNPs.

influence on the modulus improvement, that is, up to ∼50% in the cases of the SPI/glucose mass ratio of 1:0.25 and 1:0.50 but up to 400% in the case of the SPI/glucose mass ratio of 1:0.75. Furthermore, the SPI-oxidized sucrose films behaved in the mechanical properties with a tendency similar to that of SPI-oxidized glucose films. Such enhancements of the mechanical properties of the resulting SPI-OS films resulted from the curing-induced increase of cross-linking degree, corresponding to the results of sol−gel characterization (Table 2).

https://doi.org/10.1021/acsomega.1c06002
ACS Omega 2022, 7, 5883−5893

In addition, for both SPI-oxidized glucose and sucrose films, addition of 5 wt % CNPs with respect to the SPIs modified the mechanical properties of the resulting nanocomposite films. Yet, such modifications do not follow those of typical petroleum-based thermoplastic polymers reinforced with CNPs as reported in the literature.[17−22] From Tables 3 and 4, it can be found that for both uncured and cured SPI-oxidized glucose films with SPI/glucose mass ratios of 1:0.25 and 1:0.50, addition of the CNPs approximately halved both the ultimate tensile strength and Young's modulus while the strains at break of these films were enhanced significantly, that is, CNP-induced softening. However, in the case of the SPI/glucose mass ratio of 1:0.75, the effect of the CNPs on the mechanical properties of the resulting films was reversed. Such CNP-related variation can be correlated to the sol−gel test results (Table 2). It can be noticed from Table 2 that the gel fractions of both uncured and cured SPI-oxidized glucose films were decreased after addition of CNPs for the SPI/glucose mass ratio of either 1:0.25 or 1:0.50, whereas the gel fraction was increased for the SPI/glucose mass ratio of 1:0.75. Similar variations in the mechanical properties due to addition of CNPs also largely hold for both uncured and cured SPI-oxidized sucrose films. Thus, it can be concluded that addition of a small amount of CNPs can alter the cross-linking of SPIs, which further influences the mechanical properties of the resulting SPI-OS films. Figure 9 shows the TEM micrographs of the CNPs in typical SPI-oxidized glucose films, which confirms the nanosized clay particles (with the thickness lower than 100 nm) while not all the CNPs were in the full exfoliation state. Such CNPs with their ultrahigh specific surface area and aspect ratio can generate giant interphase regions between the CNPs and the SPI-OS resin even at a very small CNP mass concentration, which are responsible for the enhanced mechanical and physical properties. In addition, in all the cases of the SPI-OS films reinforced with CNPs, curing can noticeably improve their mechanical properties. For instance, for the SPI-oxidized glucose films (with the SPI/glucose mass ratio of 1:0.25) reinforced with 5 wt % CNPs with respect to the SPIs, the average ultimate tensile strength and Young's modulus prior to curing are 6.80 and 272.73 MPa, respectively, and they were enhanced up to 9.57 and 431.00 MPa, respectively, after curing. Correspondingly, the values of strain at break and toughness were reduced from 15.36% and 95.97 J/m^3 prior to curing to 10.00% and 75.84 J/m^3 after curing, respectively, that is, curing-induced brittleness of the CNP-reinforced SPI-OS films. It can also be found from Figure 4 that, with the increase of oxidized sugars up to certain levels (e.g., the SPI/sugar mass ratio of 1:0.50 in this study), the SPI-OS films became rather compliant. Furthermore, addition of a small amount of CNPs into the SPI-OS films can further magnify such a softening effect. As a result, glucose and sucrose as the two main sugar constituents of deflated soy flours can be oxidized in aqueous solution as plasterers to self-cross-link SPIs for producing soy protein composites, and CNPs can be further employed as the low-cost nanoreinforcing phase to enhance and tune the mechanical properties of the resulting CNP-reinforced SPI-OS composites.

CONCLUSIONS

In this experimental study, a green synthesis scheme has been successfully adopted to oxidize glucose and sucrose in aqueous solutions (acidified H_2O_2 solution) for preparing SPI-OS nanocomposite films. Three SPI/sugar mass ratios of 1:0.25, 1:0.50, and 1:0.75 have been considered to examine their effects on the cross-linking process and mechanical properties of the resulting SPI-OS films before and after curing. A small quantity of CNPs can be utilized for tuning the SPI cross-linking and further influencing the mechanical properties of the resulting SPI-OS clay nanocomposite films. Detailed FTIR and color and sol−gel tests have been utilized for successful characterization of the curing of the SPI-OS samples qualitatively and quantitatively, which has been further correlated to the mechanical properties of the SPI-OS films. As glucose and sucrose are the main sugar constituents of defatted soy flours, the present research has demonstrated that defatted soy flours can be used as green, self-cross-linking, and self-toughening resins for the purpose of developing various soy-protein-based composites and nanocomposites for broad applications in various industrial sectors and home utilities.

AUTHOR INFORMATION

Corresponding Author

Xiang-Fa Wu − *Department of Mechanical Engineering, North Dakota State University, Fargo, North Dakota 58108, United States;* orcid.org/0000-0003-2008-7564; Phone: +1-701-231-8836; Email: xiangfa.wu@ndsu.edu; Fax: +1-701-231-8913

Authors

Marta Bukartyk − *Department of Mechanical Engineering, North Dakota State University, Fargo, North Dakota 58108, United States; Department of Organic Chemistry, Lviv Polytechnic National University, Lviv 79069, Ukraine;* orcid.org/0000-0001-7826-0417

Oksana Zholobko − *Department of Mechanical Engineering, North Dakota State University, Fargo, North Dakota 58108, United States*

Complete contact information is available at: https://pubs.acs.org/10.1021/acsomega.1c06002

Author Contributions

The manuscript was written through contributions of the three authors.

Notes

The authors declare no competing financial interest.

ACKNOWLEDGMENTS

The financial support of this research by the North Dakota Corn Utilization Council (Award No. FAR0032332), and the DOE is gratefully acknowledge.

REFERENCES

(1) www.soynewuses.org (accessed 2021-05-15).

(2) Song, F.; Tang, D. L.; Wang, X. L.; Wang, Y. Z. Biodegradable soy protein isolated-based materials: A review. *Biomacromolecules* **2011**, *12*, 3369−3380.

(3) Koshy, R. R.; Mary, S. K.; Thomas, S.; Pothan, L. A. Environmental friendly green composites based on soy protein isolate − A review. *Food Hydrocolloids* **2015**, *50*, 174−192.

(4) Kumar, R.; Choudhary, V.; Mishra, S.; Varma, I. K.; Mattiason, B. Adhesives and plastics based on soy protein products. *Ind. Crops Prod.* **2002**, *16*, 155−172.

(5) Vnučec, D.; Kutnar, A.; Goršek, A. Soy-based adhesives for wood-bonding-a review. *J. Adhes. Sci. Technol.* **2017**, *31*, 910−931.

(6) Zink, J.; Wyrobnik, T.; Prinz, T.; Schmid, M. Physical, chemical and biochemical modification of protein-based films and coatings: An extensive review. *Int. J. Molecular Sci.* **2016**, *17*, 1376.

(7) Gu, W.; Liu, X.; Gao, Q.; Gong, S.; Li, J.; Shi, S. Q. Multiple hydrogen bonding enables strong, tough, and recyclable soy protein films. *ACS Sustainable Chem. Eng.* **2020**, *8*, 7680−7689.
(8) Pang, H.; Wang, Y.; Chang, Z.; Xia, C.; Han, C.; Liu, H.; Li, J.; Zhang, S.; Cai, L.; Huang, Z. Soy meal adhesive with high strength and water resistance via carboxymethylated wood fiber-induced crosslink. *Cellulose* **2021**, *28*, 3569−3584.
(9) Mo, X.; Sun, X. Plasticization of soy protein polymer by polyol-based plasticizers. *J. Am. Oil Chem. Soc.* **2002**, *79*, 197−201.
(10) Chen, N.; Zheng, P.; Zeng, Q.; Lin, Q.; Rao, J. Characterization and performance of soy-based adhesives cured with epoxy resin. *Polymers* **2017**, *9*, 514.
(11) Qiu, K.; Netravali, A. N. Fabrication and characterization of biodegradable composites based on microfibrillated cellulose and polyvinyl alcohol. *Compos. Sci. Technol.* **2012**, *72*, 1588−1594.
(12) Chabba, S.; Netravali, A. N. 'Green' composites part 1: Characterization of flax fabric and glutaraldehyde modified soy protein concentrate composites. *J. Mater. Sci.* **2005**, *40*, 6263−6273.
(13) Kim, J. T.; Netravali, A. N. Mechanical, thermal, and interfacial properties of green composites with ramie fiber and soy resins. *J. Agric. Food Chem.* **2010**, *58*, 5400−5407.
(14) Huang, X.; Netravali, A. N. Characterization of nano-clay reinforced phytagel-modified soy protein concentrated resin. *Biomacromolecules.* **2006**, *7*, 2783−2789.
(15) Huang, X.; Netravali, A. N. Environmentally friendly green materials from plant-based recourses: Modification of soy protein using gellan and micro/nano-fibrillated cellulose. *J. Macromol. Sci., Part A: Pure Appl. Chem.* **2008**, *45*, 899−906.
(16) Ghosh Dastidar, T.; Netravali, A. N. A soy flour based thermoset resin without the use of any external crosslinker. *Green Chem.* **2013**, *15*, 3243.
(17) Koo, J. H. *Polymer Nanocomposites: Processing, Characterization, and Applications*; McGraw Hill Co.: New York, NY, 2006.
(18) Usuki, A.; Kojima, Y.; Kawasumi, M.; Okada, A.; Fukushima, Y.; Kurauchi, T.; Kamigaito, O. Synthesis of nylon 6-clay hybrid. *J. Mater. Res.* **1993**, *8*, 1179−1184.
(19) Kojima, Y.; Usuki, A.; Kawasumi, M.; Okada, A.; Kurauchi, T.; Kamigaito, O. Synthesis of nylon 6−clay hybrid by montmorillonite intercalated with ϵ-caprolactam. *J. Polym. Sci., Part A: Polym. Chem.* **1993**, *31*, 983−986.
(20) Tjong, S. C. Structural and mechanical properties of polymer nanocomposites. *Mater. Sci. Eng. R: Rep.* **2006**, *53*, 73−197.
(21) Paul, D. R.; Robeson, L. M. Polymer nanotechnology: Nanocomposites. *Polymer* **2008**, *49*, 3187−3204.
(22) Alexandre, M.; Dubois, P. Polymer-layered silicate nanocomposites: Preparation, properties and uses of a new class of materials. *Mater. Sci. Eng. R: Rep.* **2000**, *28*, 1−63.
(23) Tucker, C. L., III; Liang, E. Stiffness predictions for unidirectional short-fiber composites: Review and evaluation. *Compos. Sci. Technol.* **1999**, *59*, 655−671.
(24) Tsai, J.; Sun, C. Effect of platelet dispersion on the load transfer efficiency in nanoclay composites. *J. Compos. Mater.* **2004**, *38*, 567−579.
(25) Weon, J. I.; Sue, H. J. Effects of clay orientation and aspect ratio on mechanical behavior of nylon-6 nanocomposite. *Polymer* **2005**, *46*, 6325−6334.
(26) Dong, Y.; Bhattacharyya, D. A simple micromechanical approach to predict mechanical behaviour of polypropylene/organo-clay nanocomposites based on representative volume element (RVE). *Comput. Mater. Sci.* **2010**, *49*, 1−8.
(27) Rahman, A.; Wu, X. F. Computational study of the effects of processing parameters on the nonlinear elastoplastic behavior of polymer nanoclay composites. *J. Compos. Sci.* **2017**, *1*, 16.
(28) Chowdhury, U.; Wu, X. F. Cohesive zone modeling of the elastoplastic and failure behavior of polymer nanoclay composites. *J. Compos. Sci.* **2021**, *5*, 131.
(29) Swain, S. K.; Priyadarshini, P. P.; Patra, S. K. Soy protein/clay bionanocomposites as ideal packaging materials. *Polym. Plastics. Technol. Eng.* **2012**, *51*, 1282−1287.
(30) Jin, M.; Ikeda, S.; Zhong, Q. Strengthening soy protein hydrogels filled with protein-coated montmorillonite nanoclay by glutaraldedyde crosslinking. *Food Sci. Technol.* **2013**, *51*, 23−29.
(31) Wu, X. F.; Dzenis, Y. A. Rate effects on mode-I delamination toughness of a graphite/epoxy laminated composite. *Int. J. Fract.* **2001**, *112*, L9−L12.
(32) Wu, X. F.; Dzenis, Y. A. Experimental determination of probabilistic edge-delamination of a graphite-fiber/epoxy composite. *Compos. Struct.* **2005**, *70*, 100−108.
(33) Zholobko, O.; Wu, X. F.; Zhou, Z.; Aulich, T.; Thakare, J.; Hurley, J. A comparative experimental study of the hygroscopic and mechanical behaviors of electrospun nanofiber membranes and solution-cast films of polybenzimidazole. *J. Appl. Polym. Sci.* **2020**, *137*, 49639.
(34) Wu, X. F.; Zholobko, O. Experimental study of the probabilistic fatigue residual strength of a carbon fiber-reinforced polymer matrix composite. *J. Compos. Sci.* **2020**, *4*, 173.
(35) Kong, J.; Yu, S. Fourier transform infrared spectroscopic analysis of protein secondary structures. *Acta Biochim. Biophys. Sin.* **2007**, *39*, 549−559.
(36) Chen, J.; Chen, X.; Zhu, Q.; Chen, F.; Zhao, X.; Ao, Q. Determination of the domain structure of the 7S and 11S globulins from soy proteins by XRD and FTIR. *J. Sci. Food Agric.* **2013**, *93*, 1687−1691.
(37) Huang, X.; Netravali, A. N. Characterization of Nano-Clay Reinforced Phytagel-Modified Soy Protein Concentrate Resin. *Biomacromolecules* **2006**, *7*, 2783−2789.
(38) Ogale, A. A.; Cunningham, P.; Dawson, P. L.; Acton, J. C. Viscoelastic thermal and microstructural characterization of soy protein isolate films. *J. Food Sci.* **2000**, *65*, 672−679.
(39) Swain, S. N.; Rao, K. K.; Nayak, P. L. Biodegradable polymers: IV. Spectral, thermal, and mechanical properties of cross-linked soy protein concentrate. *Polym. Int.* **2005**, *54*, 739−743.
(40) https://www.netzsch-thermal-analysis.com/us/materials-applications/us-applications/thermal-decomposition-of-glucose/ (accessed 2021-05-15).
(41) Bednarek, P.; Szafran, M. Thermal decomposition of monosaccharides derivatives applied in ceramic gelcasting process investigated by the coupled DTA/TG/MS analysis. *J. Therm. Anal. Calorim.* **2012**, *109*, 773−782.
(42) Ash, B. J.; Stone, J.; Rogers, D. F.; Schadler, L. S.; Siegel, R. W.; Benicewicz, B. C.; Apple, T. Investigation into the thermal and mechanical behavior of PMMA/alumina nanocomposites. *MRS Proc.* **2000**, *661*, 10.
(43) Cuney, S.; Gérard, J. F.; Pascault, J. P.; Vigier, G. Organic-rich hybrid O/I systems based on isocyanate chemistry. *Mater. Res. Soc. Symp. Proc.* **1996**, *435*, 143.
(44) Ash, B. J.; Schadler, L. S.; Siegel, R. W. Glass transition behavior of alumina/polymethylmethacrylate nanocomposites. *Mater. Lett.* **2002**, *55*, 83−87.

https://doi.org/10.1021/acsomega.1c06002
ACS Omega 2022, 7, 5883−5893